

Correlated Chern insulators in two-dimensional Raman lattices: A cold-atom regularization of strongly coupled four-Fermi field theories

L. Ziegler¹, E. Tirrito^{2,3}, M. Lewenstein^{3,4}, S. Hands⁵ and A. Bermudez^{1,6}

¹Departamento de Física Teórica, Universidad Complutense, 28040 Madrid, Spain

²International School for Advanced Studies (SISSA), via Bonomea 265, 34136 Trieste, Italy

³ICFO - Institut de Ciències Fotoniques, Barcelona Institute of Science and Technology, Avenida Carl Friedrich Gauss 3, 08860 Castelldefels (Barcelona), Spain

⁴ICREA, Lluís Companys 23, 08010 Barcelona, Spain

⁵Department of Physics, Faculty of Science and Engineering, Swansea University, Singleton Park, Swansea SA28PP, United Kingdom

⁶Instituto de Física Teórica, UAM-CSIC, Universidad Autónoma de Madrid, Cantoblanco, 28049 Madrid, Spain



(Received 22 December 2020; revised 8 July 2022; accepted 25 July 2022; published 20 October 2022)

We show that synthetic spin-orbit coupling for ultracold atoms in optical Raman potentials can be exploited to build versatile quantum simulators of correlated Chern insulators connected to strongly coupled four-Fermi field theories similar to the Gross-Neveu model in $(2 + 1)$ dimensions. Exploiting this multidisciplinary perspective, we identify a large- N quantum anomalous Hall (QAH) effect in absence of any external magnetic field, and use it to delimit regions in parameter space where these correlated topological phases appear, the boundaries of which are controlled by strongly coupled fixed points of these four-Fermi relativistic field theories. We further show how, for strong interactions, the QAH effect gives way to magnetic phases described by a two-dimensional quantum compass model in a transverse field. We present a detailed description of the phase diagram using the large- N effective potential, and variational techniques such as projected entangled pairs.

DOI: [10.1103/PhysRevResearch.4.L042012](https://doi.org/10.1103/PhysRevResearch.4.L042012)

Special relativity and quantum mechanics predict the coupling of the intrinsic angular momentum of the electron with its own motion, yielding the fine structure of atomic spectra [1]. This *spin-orbit coupling* (SOC) is intimately related to relativistic quantum field theories (QFTs) via Dirac's equation [2,3] and, ultimately, quantum electrodynamics [4]. Indeed, it is the comparison of perturbative calculations of this weakly coupled QFT [5,6] with high-precision measurements of the intrinsic magnetic moment of the electron [7] and the fine structure constant [8] that yields one of the most stringent tests of a physical theory to date.

SOC is also a cornerstone of modern condensed matter [9,10], underlying the discovery [11–15] of a topological mechanism for the ordering of matter [16–18]. Chern insulators [19–21], characterized by a nonzero topological invariant at the bulk and by current-carrying states at the boundaries, epitomize this ordering mechanism. It is remarkable that elaborate concepts of algebraic topology [22], i.e., Chern numbers [23] of the Bloch bundle, lead to the quantization of the Hall conductivity in absence of external magnetic fields. This so-called quantum anomalous Hall (QAH) effect [24,25] may have promising technological applications [26].

These two consequences of SOC are very well understood: Chern insulators employ free-electron band-structure calculations, while quantum electrodynamics uses perturbation theory about a weakly coupled fixed point. However, open questions arise as one abandons these limits to explore (i) *correlated Chern insulators* for strong SOC and interparticle interactions, and (ii) relativistic QFTs with SOC controlled by nonperturbative strongly coupled fixed points. As shown below, these two topics can be connected by considering SOC in light of specific discretizations [27] of *strongly coupled four-Fermi QFTs* [28–30]. Originally introduced by Fermi for the weak interactions [31], four-Fermi QFTs such as the Nambu-Jona-Lasinio [32] or Gross-Neveu (GN) [33] models are nowadays considered as effective QFTs for the strong interactions. We show that, working in $(2 + 1)$ dimensions and dispensing with the notion of chirality, a Hubbard model [34] with strong SOC leads to analogous four-Fermi QFTs with ground states corresponding to correlated Chern insulators.

Leveraging this connection, we develop nonperturbative studies of Chern insulators following two strategies: (i) Viewing the lattice as an artificial regularization [35], we exploit the lattice-field-theory machinery [36] to connect the quantum phase transitions delimiting the correlated Chern insulators to strongly coupled fixed points. (ii) Considering experimental setups where the lattice is real, and the SOC and four-Fermi interactions appear naturally, such as Fermi gases with synthetic SOC in optical lattices [37,38], we obtain a physical regularization of strongly coupled QFTs that serve as quantum simulators for a correlated QAH effect [39–41].

Published by the American Physical Society under the terms of the [Creative Commons Attribution 4.0 International](https://creativecommons.org/licenses/by/4.0/) license. Further distribution of this work must maintain attribution to the author(s) and the published article's title, journal citation, and DOI.

The model. We consider a Wilsonian discretization [27] of a Hamiltonian QFT for N flavors of self-interacting Dirac fields $\{\psi_f(\mathbf{x})\}_{f=1}^N$ which, in natural units $\hbar = c = 1$, reads

$$H = a_1 a_2 \sum_{\mathbf{x} \in \Lambda_s} \left\{ \sum_{j=1,2} \left[-\bar{\Psi}(\mathbf{x}) \left(\frac{i\gamma^j}{2a_j} + \frac{r_j}{2a_j} \right) \Psi(\mathbf{x} + a_j \mathbf{e}_j) + \bar{\Psi}(\mathbf{x}) \left(\frac{m}{4} + \frac{r_j}{2a_j} \right) \Psi(\mathbf{x}) + \text{H.c.} \right] - \frac{g^2}{2N} \left(\bar{\Psi}(\mathbf{x}) \Psi(\mathbf{x}) \right)^2 \right\}, \quad (1)$$

where the vector $\Psi(\mathbf{x}) = (\psi_1(\mathbf{x}), \dots, \psi_N(\mathbf{x}))^t$ is composed of N spinor fields, $\bar{\Psi}(\mathbf{x}) = (\psi_1^\dagger(\mathbf{x})\gamma^0, \dots, \psi_N^\dagger(\mathbf{x})\gamma^0)$ is the adjoint, and $\gamma^0, \gamma^1, \gamma^2$ are the gamma matrices for a $(2+1)$ -dimensional spacetime $\{\gamma^\mu, \gamma^\nu\} = 2g^{\mu\nu}\mathbb{I}$ with $g^{\mu\nu} = \text{diag}(1, -1, -1)$ and spacetime indexes $\mu, \nu \in \{0, 1, 2\}$. Here, only the spatial coordinates are discretized [42] with lattice spacings a_1, a_2 , yielding $\Lambda_s = \{\mathbf{x} = n_1 a_1 \mathbf{e}_1 + n_2 a_2 \mathbf{e}_2, \forall (n_1, n_2) \in \mathbb{Z}_{N_1} \times \mathbb{Z}_{N_2}\}$. In Eq. (1), we have also introduced the Wilson parameters $\{r_j\}$, a bare mass m , and a coupling g^2 controlling the simplest Lorentz-invariant interparticle interaction. In the long-wavelength limit, one obtains 4 fermion doublers [43,44], each described by a continuum Dirac field $\{\Psi_{n_d}(\mathbf{x})\}_{n_d}$, $\mathbf{n}_d = (n_{d,1}, n_{d,2}) \in \{0, 1\} \times \{0, 1\}$ with a different bare mass

$$m_{n_d} = m + 2n_{d,1}r_1/a_1 + 2n_{d,2}r_2/a_2. \quad (2)$$

Let us discuss the connection of Eq. (1) to SOC. In $(2+1)$ dimensions, one can choose 2×2 gamma matrices, such that the spinor representation of rotations allows us to interpret the components $\psi_{f,1}(\mathbf{x})$ [$\psi_{f,2}(\mathbf{x})$] as spin up (down) fermions. If one chooses $\gamma^0 = \sigma^z$, $\gamma^1 = i\sigma^x$, $\gamma^2 = -i\sigma^y$, the spin-flip tunnelings (1), $\Psi^\dagger(\mathbf{x}) \frac{i\sigma^x}{2a_2} \Psi(\mathbf{x} + a_2 \mathbf{e}_2) - \Psi^\dagger(\mathbf{x}) \frac{i\sigma^y}{2a_1} \Psi(\mathbf{x} + a_1 \mathbf{e}_1)$, correspond to the lattice-field-theory version of Rashba SOC $\mathbf{e}_3 \cdot (\mathbf{p} \wedge \boldsymbol{\sigma}) = i\sigma^x \partial_y - i\sigma^y \partial_x$ [9], where the derivatives are discretized by finite differences on adjacent lattice sites. Other basis of gamma matrices lead to variants of this SOC [38]. We note that, in contrast to $(2+1)$ -dimensional Gross-Neveu models [28], where discrete chiral symmetry $\Psi(\mathbf{x}) \rightarrow \gamma^5 \Psi(\mathbf{x})$ can be enforced by using 4-component spinors, there is no chirality in our case as $\gamma^5 = i\gamma^0 \gamma^1 \gamma^2 = -\mathbb{I}$.

Quantum simulator. We now map the couplings of the single-flavor Hamiltonian (1) in the standard Dirac basis $\gamma^0 = \sigma^z$, $\gamma^1 = i\sigma^y$, $\gamma^2 = -i\sigma^x$ to the experimental parameters of ultracold atoms in *Raman optical lattices* [45–47]. To get a fully tunable quantum simulator of Eq. (1) in this basis, we generalize the SOC scheme of [48,49], such that atoms in two states $\{|\uparrow\rangle, |\downarrow\rangle\}$ are subjected to the periodic potential

$$V = \frac{V_{0,1}}{2} \cos^2(kx_1) \mathbb{I}_2 + \frac{\tilde{V}_{0,1}}{2} \cos kx_1 e^{i(kx_2 - \Delta\omega t - \phi_1)} \sigma^+ + \frac{V_{0,2}}{2} \cos^2(kx_2) \mathbb{I}_2 + \frac{\tilde{V}_{0,2}}{2} \cos kx_2 e^{i(kx_1 - \Delta\omega t - \phi_2)} \sigma^+ + \text{H.c.} \quad (3)$$

Here, $V_{0,j}$ ($\tilde{V}_{0,j}$) stem from ac-Stark shifts (Rabi frequencies) of pairs of counterpropagating (orthogonal) laser beams with wavelength $\lambda = 2\pi/k$. The Raman term $\tilde{V}_{0,1}$ ($\tilde{V}_{0,2}$) with relative phase ϕ_1 (ϕ_2) induces a two-photon transition between the internal states $\sigma^+ = |\uparrow\rangle\langle\downarrow|$ when the laser beat note is $\Delta\omega = \omega_0 - \delta$, where ω_0 is the transition frequency and $\delta \ll \omega_0$ is the detuning. Accordingly, the periodic Raman potential

is due to processes where the atom absorbs a photon from the standing wave along the x_1 (x_2) axis, and subsequently emits it in the traveling wave along x_2 (x_1). To minimize residual photon scattering and heating, one may consider working with lanthanide [50–52] or alkali-earth [53,54] atoms.

As customary for ultracold atoms [55–57], for deep potentials $V_{0,j}, \tilde{V}_{0,j} \gg E_R = k^2/2m$, where m is the atomic mass, the dynamics can be expressed as a lattice model where atoms tunnel between neighboring potential minima, and collide in pairs with an s -wave scattering length a_s . The specific interference pattern in Eq. (3) is crucial, as it ensures that the Raman terms do not contribute with on-site spin flips, but drive instead spin-flip tunnelings along the two spatial directions with a tunable relative phase. Using a basis of Wannier functions in the single-band approximation, and working in a rotating frame with respect to the Raman terms, one finds

$$H = - \sum_{n,j} [t_j (c_{n,\uparrow}^\dagger c_{n+\mathbf{e}_j,\uparrow} + c_{n,\downarrow}^\dagger c_{n+\mathbf{e}_j,\downarrow}) + \text{H.c.}] - \sum_{n,j} [i\tilde{t}_j e^{-i\phi_{j,n}} (c_{n,\uparrow}^\dagger c_{n+\mathbf{e}_j,\downarrow} - c_{n,\downarrow}^\dagger c_{n-\mathbf{e}_j,\downarrow}) + \text{H.c.}] + \sum_n U_{\uparrow\downarrow} c_{n,\uparrow}^\dagger c_{n,\downarrow}^\dagger c_{n,\downarrow} c_{n,\uparrow} + \frac{\delta}{2} (c_{n,\uparrow}^\dagger c_{n,\uparrow} - c_{n,\downarrow}^\dagger c_{n,\downarrow}), \quad (4)$$

where the fermionic operators $c_{n,s}^\dagger$ ($c_{n,s}$) create (annihilate) an atom in state $s \in \{\uparrow, \downarrow\}$ at $\mathbf{x}_n = \sum_j (\frac{\lambda}{4} + \frac{\lambda}{2} n_j) \mathbf{e}_j$. The above Hamiltonian parameters, obtained by different overlaps of Wannier functions, lead to spin-independent tunnelings $t_j = 4(E_R/\sqrt{\pi})(V_{0,j}/E_R)^{3/4} e^{-2\sqrt{V_{0,j}/E_R}}$, and contact Hubbard interactions $U_{\uparrow\downarrow} = \sqrt{8/\pi} k_0 a_s E_R (V_{0,1} V_{0,2}/E_R^2)^{1/4}$. Using a Gaussian approximation for the Wannier functions, we obtain a spin-flip tunneling along the x_j axis with strength $\tilde{t}_j = \tilde{V}_{0,j} e^{-(\pi^2/4)\sqrt{V_{0,j}/E_R}}$ and phase $\phi_{j,n} = \phi_j - \pi(n_1 + n_2)$.

To find the mapping of Eq. (4) to Eq. (1), we rescale the atomic operators and perform a gauge transformation $\psi_1(\mathbf{x}_n) = c_{n,\uparrow}/\sqrt{a_1 a_2}$, $\psi_2(\mathbf{x}_n) = e^{i\pi(n_1+n_2)} c_{n,\uparrow}/\sqrt{a_1 a_2}$. Setting the Raman-beam phases to $\phi_1 = 0, \phi_2 = \pi/2$, we find that model (4) maps to the lattice field theory (1) for $N = 1$ with

$$a_j = \frac{1}{2\tilde{t}_j}, \quad r_j = \frac{t_j}{\tilde{t}_j}, \quad m = \frac{\delta}{2} - 2(t_1 + t_2), \quad g^2 = \frac{U_{\uparrow\downarrow}}{4\tilde{t}_1 \tilde{t}_2}. \quad (5)$$

We note that the anisotropic lattice spacings of the field theory (1) are mapped onto the atomic tunneling strengths, not to the optical-lattice spacing $\lambda/2$. Therefore, the continuum limit does not require modifying the laser wavelength $\lambda \rightarrow 0$, but instead setting the experimental parameters ($t_j, \tilde{t}_j, \delta, U_{\uparrow\downarrow}$) to certain values, such that the bare couplings (m, a_j, r_j, g^2) lie

in the vicinity of a critical point. Here, the energy gap is very small $\Delta\epsilon \ll \tilde{t}_j$, and the relevant length scale ξ is much larger than the lattice spacing $\xi \propto 1/\Delta\epsilon \gg a_j$, such that a continuum coarse-grained QFT can capture the low-energy physics.

Large- N QAH effect. In the noninteracting $g^2 = 0$ and isotropic $a_1 = a_2 =: a$, $r_1 = r_2 = 1$ limits, the single-flavor Hamiltonian (1) corresponds to a square-lattice version [20,21] of Haldane's model [19,58] of the QAH effect [25]. This model has been realized in semiconducting ferromagnetic films [59,60], observing a quantized Hall conductance for vanishing magnetic fields. Regarding Eq. (1), this quantization depends on the Chern number via

$$\sigma_{xy} = \frac{e^2}{h} N_{\text{Ch}}, \quad N_{\text{Ch}} = \frac{N}{2} \sum_{n_d} (-1)^{(n_{d,1} + n_{d,2})} \text{sgn}(m_{n_d}). \quad (6)$$

According to the doubler masses (2), and using Eq. (6) in the single-flavor limit $N = 1$, one finds that the Chern number is quantized to a nonzero integer $N_{\text{Ch}} = -1$ when $ma \in (-2, 0)$, whereas $N_{\text{Ch}} = +1$ when $ma \in (-4, -2)$, both of which lead to a QAH conductance, and $N_{\text{Ch}} = 0$ otherwise. Let us note, however, that interactions do not seem to play any relevant role in these semiconducting realizations [59,60]. Instead, for cold atoms with the Dirac-Wilson SOC (4), the spinor is formed by two internal states that interact naturally via such s -wave scattering. The key advantage is that the coupling g^2 , as well as all other microscopic parameters (5), can be experimentally tuned. This brings a unique opportunity to realize correlated Chern insulators with a neat connection to strongly coupled relativistic QFTs. In this context [61–67], topological insulators in different symmetry classes and dimensions [68] correspond to lower-dimensional versions of domain-wall fermions [69], where the topological invariants control a Chern-Simons-type response [21,70–72].

We now describe the fate of this QAH effect as interactions are switched on. From the analogy with the GN model [33], one expects dynamical mass generation via a scalar condensate $\Sigma_0 \propto \langle \bar{\Psi}(\mathbf{x})\Psi(\mathbf{x}) \rangle$ to arise. We note, however, that due to the particular representation of the gamma matrices, this condensate is not associated with chiral symmetry breaking as in even spacetime dimensions [33,63–67], or in odd ones with a reducible representation of the gamma matrices [28,29]. If such models are discretized following the Wilson prescription, it is well known that the fermions can also form a pseudoscalar condensate $\Pi_0 \propto \langle \bar{\Psi}(\mathbf{x})i\gamma^5\Psi(\mathbf{x}) \rangle$ through the spontaneous breakdown of parity, which also appears in situations where the interactions are mediated by a gauge field [73,74]. In contrast, we identify two π condensates, $\Pi_1 \propto \langle \bar{\Psi}(\mathbf{x})\gamma^1\Psi(\mathbf{x}) \rangle$ and $\Pi_2 \propto \langle \bar{\Psi}(\mathbf{x})\gamma^2\Psi(\mathbf{x}) \rangle$, the nonzero values of which lead instead to the spontaneous breakdown of inversion symmetry. In the language of the underlying Hubbard model (4) for a single flavor, these π condensates represent two possible ferromagnetic orderings $\Pi_1 \propto \langle f_{n,\uparrow}^\dagger f_{n,\downarrow} \rangle + \langle f_{n,\downarrow}^\dagger f_{n,\uparrow} \rangle$, and $\Pi_2 \propto i\langle f_{n,\uparrow}^\dagger f_{n,\downarrow} \rangle - i\langle f_{n,\downarrow}^\dagger f_{n,\uparrow} \rangle$.

To understand how these condensates affect the QAH, we make use of nonperturbative *large- N techniques* developed for QFTs in Euclidean spacetime $x = (it, \mathbf{x})$ [75]. Let us outline our calculation. First of all, we introduce three auxiliary scalar fields $\sigma(x)$, $\pi_1(x)$, $\pi_2(x)$, which do not propagate, but medi-

ate instead the contact four-Fermi term (1). This allows us to organize the Feynman diagrams of the QFT according to their order in N , identifying the leading contributions when $N \rightarrow \infty$ as those with a single fermion loop and an even number of external lines for the auxiliary fields. In this way, we can obtain analytically the radiative corrections to the classical potential, namely the leading-order [33,76] *effective potential* [77]. In our case, we are interested in the effective potential for $\boldsymbol{\pi}(x) = (\pi_1(x), \pi_2(x))$, the minimum of which can be used to locate the spontaneous breakdown of inversion symmetry $\boldsymbol{\Pi} := (\Pi_1, \Pi_2) = \langle \boldsymbol{\pi}(x) \rangle \neq \mathbf{0}$, $\forall x$. By resumming the diagrams to all orders of the coupling, we obtain

$$\begin{aligned} \frac{V_{\text{eff}}(\tilde{\boldsymbol{\Pi}})}{N} &= \frac{\tilde{\boldsymbol{\Pi}}^2}{2\tilde{g}^2} - \sum_k \ln \left(1 + \frac{\sum_\mu \tilde{\Pi}_\mu^2}{M_k^2 + \sum_\mu p_{\mu,k}^2} \right) \\ &\quad - \frac{1}{2} \sum_k \ln \left[1 - \left(\frac{2 \sum_\mu \tilde{\Pi}_\mu p_{\mu,k}}{M_k^2 + \sum_\mu (p_{\mu,k}^2 + \tilde{\Pi}_\mu^2)} \right)^2 \right], \end{aligned} \quad (7)$$

where we work in discretized Euclidean time with spacing a_0 and antiperiodic boundary conditions after N_0 time steps, such that the momentum lies in the Brillouin zone $k = (k_0, \mathbf{k}) \in \text{BZ} = [-\pi, \pi]^3$. Here, we have introduced a shorthand notation $\sum_k = \sum_{k \in \text{BZ}} / N_0 N_1 N_2$, $p_{\mu,k} = 2\kappa_\mu \sin k_\mu$, and $M_k = \tilde{m} + 1 - 2\kappa_\mu \cos k_\mu + \tilde{\Sigma}_0$, with $\kappa_\mu = 1/2a_\mu (\sum_v a_v^{-1})$, $r_\mu = 1$, and use dimensionless quantities [78] setting $\tilde{\Pi}_0 = 0$.

We minimize the effective potential (7) considering a homogeneous scalar condensate $\Sigma_0 = \langle \sigma(x) \rangle \forall x$, and then obtain its value through the self-consistency equation

$$\tilde{\Sigma}_0 = \tilde{g}^2 \sum_k \frac{M_k}{M_k^2 + \sum_\mu (p_{\mu,k}^2 + \tilde{\Pi}_\mu^2)}. \quad (8)$$

From this pair of equations (7) and (8), one can extract the effects of correlations on the large- N QAH effect. First, in the parity-symmetric phases without π condensates, we find a nonzero scalar condensate $\Sigma_0(g^2) \neq 0$ for any $g^2 > 0$ [79]. This condensate contributes to the static part of the fermionic self-energy $\Sigma(0, \mathbf{k}) = \Sigma_0(g^2)\gamma^0$, which is defined via $G^{-1}(ik_0, \mathbf{k}) = ik_0 - (M_k\gamma^0 + \sum_j p_{j,k}\gamma^j\gamma^j) + \Sigma(ik_0, \mathbf{k})$, and obtained from the Fourier and Matsubara transforms of the two-point function $G(x-y) = \langle T\{\Psi^\dagger(x)\Psi(y)\} \rangle$. Remarkably, the static self-energy can be used for a practical calculation [80–83] of topological invariants [84,85] beyond the noninteracting limit [86]. In our case, we obtain a closed expression for the dependence of the Chern number on the interaction strength

$$N_{\text{Ch}}(g^2) = \frac{N}{2} \sum_{n_d} (-1)^{(n_{d,1} + n_{d,2})} \text{sgn}[m_{n_d} + \Sigma_0(g^2)], \quad (9)$$

which predicts the existence of correlated phases where the interacting fermions still display a quantized Hall conductivity $\sigma_{xy} = \pm \frac{e^2}{h} N$. These regions, depicted in Fig. 1, show that the QAH effect survives for considerably large interactions.

Let us now discuss the π condensation, which occurs via two possible channels: $(\Pi_1, 0)$ for $a_1 > a_2$, or $(0, \Pi_2)$ for $a_1 < a_2$, each of which corresponds to orthogonal ferromagnetic orders [87]. As clarified below, this differs from the

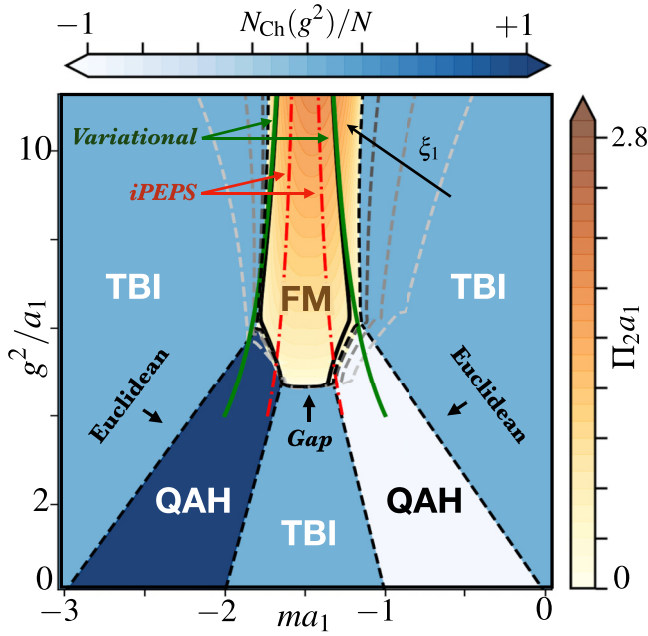


FIG. 1. Phase diagram of the four-Fermi QFT. Contour plots of the Chern number N_{Ch} (blue) and π condensate (orange) for $a_2 = 2a_1$, predicting large- N QAH phases, trivial band insulators (TBIs), and a ferromagnetic phase (FM). These phases are separated by dashed lines (Euclidean) obtained from Eqs. (7) and (8) in gray scale with an increasing timelike anisotropy $\xi_1 = a_1/a_0 \in \{10, 20, 40, 64\}$. The black solid line is obtained by solving self-consistent equations (Gap) in the time-continuum limit $a_0 \rightarrow 0$, which can only delimit the area of the FM but give no further information about the TBI or QAH phases. The green solid lines (Variational) represent the product-state prediction for the compass model (12), and the red dashed-dotted lines correspond to iPEPs.

standard ferromagnetism in solid-state materials as, in particular, we find that low-energy excitations are gapped. The set of parameters where the π condensates form define critical lines separating the correlated QAH phases from long-range-ordered ferromagnets (FMs), as depicted in Fig. 1. From a closer analysis of the effective potential, we note that these critical lines describe second-order quantum phase transitions which, interestingly, become first-order around the central region. This will be discussed in detail in future work.

Quantum compass model and projected-entangled pairs.

The above results have unveiled a rich phase diagram with correlated Chern insulators, trivial band insulators, and ferromagnetic parity-broken phases, separated by critical lines related to the specific values of σ and π condensates, and controlled by strongly coupled QFTs. However, these predictions are strictly valid in the $N \rightarrow \infty$ limit, whereas the cold-atom realization (4) yields $N = 1$. Although future experiments could validate whether our large- N predictions survive in the ultimate quantum limit of $N = 1$, exploring the characteristic scaling of the strongly coupled fixed points, it would be reassuring to have a partial independent confirmation.

Exploiting the connection of the four-Fermi field theory (1) to the Hubbard model with SOC (4), we can derive an effective description for $\tilde{g}^2 \gg 1$ via Anderson's exchange [88,89]. This limit is governed by second-order processes,

where fermions tunnel back and forth forming virtual double occupancies. In contrast to the standard Hubbard model, where this leads to Heisenberg interactions [90], we obtain

$$H_{\text{eff}} = \sum_{x \in \Lambda_s} (J_x \tau_x^x \tau_{x+a_2 e_2}^x + J_y \tau_x^y \tau_{x+a_1 e_1}^y - h \tau_x^z). \quad (10)$$

Here, the bilinears $\{\tau_x^\alpha = a_1 a_2 \Psi^\dagger(x) \sigma^\alpha \Psi(x)\}_{\alpha=x,y,z}$ yield spin-1/2 operators $\mathbf{S}_x = \frac{1}{2} \boldsymbol{\tau}_x$ when each site is occupied by a single fermion. The exchange couplings obtained read

$$J_x = -\frac{a_1}{2a_2 g^2} = -\frac{2\tilde{t}_2^2}{U_{\uparrow\downarrow}}, \quad J_y = -\frac{a_2}{2a_1 g^2} = -\frac{2\tilde{t}_1^2}{U_{\uparrow\downarrow}}, \quad (11)$$

whereas $h = (m + a_1^{-1} + a_2^{-2})$ is an effective transverse field. This spin model belongs to the family of *quantum compass models* (QCMs) [91], which have a characteristic directionality of the spin-spin interactions responsible for the appearance of topologically ordered phases of matter with anyonic excitations in the honeycomb lattice [92]. For our rectangular lattice, the QCM has been thoroughly studied for $h = 0$ [91], where gaugelike symmetries [93] enforce a 2-fold degeneracy of the eigenstates, and can be exploited to encode a logical qubit for fault-tolerant quantum computing [94,95]. As one tunes the couplings across the symmetric point $J_x = J_y$, a first-order phase transition between two gapped ferromagnetic orders occurs [96–98], i.e., $\langle \tau_x^x \rangle \neq 0$ when $J_x > J_y$, and $\langle \tau_x^y \rangle \neq 0$ when $J_x < J_y$.

In contrast to the zero-field case, the transverse-field QCM remains largely unexplored. Note that the above order parameters correspond exactly to the previously introduced π condensates which, according to our large- N results, may also appear for $h \neq 0$. We have performed a variational study of the model using two *Ansätze*. The first *Ansatz* is a simple product state where all spins point in a given direction along the equatorial plane. It allows us to predict two types of second-order phase transitions with the following orderings:

$$\begin{aligned} \langle \tau_x^x \rangle = \Pi_1 &= \left(1 - \frac{h^2}{4J_x^2}\right)^{1/2}, & \text{if } 2|J_x| \geq |h|, J_y > J_x, \\ \langle \tau_x^y \rangle = \Pi_2 &= \left(1 - \frac{h^2}{4J_y^2}\right)^{1/2}, & \text{if } 2|J_y| \geq |h|, J_y < J_x. \end{aligned} \quad (12)$$

The ground state displays a $\Pi_1 \propto \langle \tau_x^x \rangle$ ($\Pi_2 \propto \langle \tau_x^y \rangle$) condensate for $J_x < J_y < 0$ ($J_y < J_x < 0$) which, according to Eq. (11), occurs for $a_1 > a_2$ ($a_1 < a_2$) in agreement with the large- N results. These critical lines are compared to the large- N prediction in Fig. 1, showing a remarkable agreement.

The second *Ansatz* is based on infinite projected-entangled pairs (iPEPS) [99–101], a powerful framework for the classical simulation of 2D strongly correlated models that captures the interplay of locality and entanglement by expressing an entangled many-body wave function in terms of local tensors [102]. In Fig. 1 (red line), we present the results for $D = 2$ obtained by locating the divergence of the magnetic susceptibility $\chi_j = \partial M_j / \partial h$. As shown in [98] for the $h = 0$ model, iPEPS with $D = 2$ already yields better results than those obtained by combining fermionization with mean-field

theory. We have checked that, for $h \neq 0$, iPEPS also provides significantly lower variational energies than the ones obtained by large- N or the product-state *Ansatz*. This has allowed us to draw a more accurate prediction with a clear displacement of the critical lines and a narrower FM region.

Conclusions. We have shown that 2D Hubbard models with SOC, which can be realized with neutral atoms in Raman lattices, give access to the ultimate quantum limit of strongly coupled QFTs hosting correlated Chern insulators and displaying a QAH effect. The framework hereby presented can serve as the stepping stone to address open questions, such as finite fermion densities in searching for cold-atom realizations of fractional QAH effects [103,104] and contemporary relativistic QFTs with fractionalization [105].

Acknowledgments. We are very grateful to Luca Tagliacozzo for fruitful discussions. This project has received funding from the European Union's Horizon 2020 research and innovation program under the Marie

Skłodowska-Curie Grant Agreement No. 665884, the Spanish Ministry MINECO (National Plan 15 Grant: FISICATEAMO No. FIS2016-79508-P, SEVERO OCHOA No. SEV-2015-0522, FPI), European Social Fund, Fundació Cellex, Generalitat de Catalunya (AGAUR Grant No. 2017 SGR 1341, CERCA/Program), ERC AdG NOQIA, EU FEDER, and the National Science Centre, Poland-Symfonia Grant No. 2016/20/W/ST4/00314. The work of S.J.H. was supported by STFC Grant No. ST/L000369/1. A.B. acknowledges support from the Ramón y Cajal program RYC-2016-20066, CAM/FEDER Project S2018/TCS-4342 (QUITEMADCM), and PGC2018-099169-B-I00 (MCIU/AEI/FEDER, UE), from the Grant IFT Centro de Excelencia Severo Ochoa CEX2020-001007-S, funded by MCIN/AEI/10.13039/501100011033, and from the CSIC Research Platform on Quantum Technologies PTI-001. S.H. is supported by STFC Grant No. ST/T000813/1. A.B. acknowledges support from PID2021-127726NB-I00.

-
- [1] L. H. Thomas, The motion of the spinning electron, *Nature* **117**, 514 (1926).
- [2] P. A. M. Dirac, The quantum theory of the electron, *Proc. R. Soc. London, Ser. A* **117**, 610 (1928).
- [3] P. A. M. Dirac, A theory of electrons and protons, *Proc. R. Soc. London, Ser. A* **126**, 360 (1930).
- [4] S. S. Schweber, *QED and the Men Who Made It: Dyson, Feynman, Schwinger, and Tomonaga* (Princeton University Press, Princeton, 1994).
- [5] J. Schwinger, On quantum-electrodynamics and the magnetic moment of the electron, *Phys. Rev.* **73**, 416 (1948).
- [6] T. Aoyama, M. Hayakawa, T. Kinoshita, and M. Nio, Tenth-Order QED Contribution to the Electron $g-2$ and an Improved Value of the Fine Structure Constant, *Phys. Rev. Lett.* **109**, 111807 (2012).
- [7] D. Hanneke, S. Fogwell, and G. Gabrielse, New Measurement of the Electron Magnetic Moment and the Fine Structure Constant, *Phys. Rev. Lett.* **100**, 120801 (2008).
- [8] R. H. Parker, C. Yu, W. Zhong, B. Estey, and H. Müller, Measurement of the fine-structure constant as a test of the standard model, *Science* **360**, 191 (2018).
- [9] Y. A. Bychkov and E. I. Rashba, Oscillatory effects and the magnetic susceptibility of carriers in inversion layers, *J. Phys. C* **17**, 6039 (1984).
- [10] G. Dresselhaus, Spin-orbit coupling effects in zinc blende structures, *Phys. Rev.* **100**, 580 (1955).
- [11] C. L. Kane and E. J. Mele, Z_2 Topological Order and the Quantum Spin Hall Effect, *Phys. Rev. Lett.* **95**, 146802 (2005).
- [12] C. L. Kane and E. J. Mele, Quantum Spin Hall Effect in Graphene, *Phys. Rev. Lett.* **95**, 226801 (2005).
- [13] B. A. Bernevig, T. L. Hughes, and S.-C. Zhang, Quantum spin Hall effect and topological phase transition in HgTe quantum wells, *Science* **314**, 1757 (2006).
- [14] M. König, S. Wiedmann, C. Brune, A. Roth, H. Buhmann, L. W. Molenkamp, X.-L. Qi, and S.-C. Zhang, Quantum spin Hall insulator state in HgTe quantum wells, *Science* **318**, 766 (2007).
- [15] D. Hsieh, D. Qian, L. Wray, Y. Xia, Y. S. Hor, R. J. Cava, and M. Z. Hasan, A topological dirac insulator in a quantum spin Hall phase, *Nature (London)* **452**, 970 (2008).
- [16] M. Z. Hasan and C. L. Kane, Colloquium: Topological insulators, *Rev. Mod. Phys.* **82**, 3045 (2010).
- [17] X.-L. Qi and S.-C. Zhang, Topological insulators and superconductors, *Rev. Mod. Phys.* **83**, 1057 (2011).
- [18] C.-K. Chiu, J. C. Y. Teo, A. P. Schnyder, and S. Ryu, Classification of topological quantum matter with symmetries, *Rev. Mod. Phys.* **88**, 035005 (2016).
- [19] F. D. M. Haldane, Model for a Quantum Hall Effect without Landau Levels: Condensed-Matter Realization of the "Parity Anomaly", *Phys. Rev. Lett.* **61**, 2015 (1988).
- [20] X.-L. Qi, Y.-S. Wu, and S.-C. Zhang, Topological quantization of the spin Hall effect in two-dimensional paramagnetic semiconductors, *Phys. Rev. B* **74**, 085308 (2006).
- [21] X.-L. Qi, T. L. Hughes, and S.-C. Zhang, Topological field theory of time-reversal invariant insulators, *Phys. Rev. B* **78**, 195424 (2008).
- [22] M. Nakahara, *Geometry, Topology and Physics* (CRC Press, Bristol and Philadelphia, 2018).
- [23] S.-S. Chern, Characteristic classes of Hermitian manifolds, *Ann. Math.* **47**, 85 (1946).
- [24] F. D. M. Haldane, Nobel lecture: Topological quantum matter, *Rev. Mod. Phys.* **89**, 040502 (2017).
- [25] C.-X. Liu, S.-C. Zhang, and X.-L. Qi, The quantum anomalous hall effect: Theory and experiment, *Annu. Rev. Condens. Matter Phys.* **7**, 301 (2016).
- [26] A. Soumyanarayanan, N. Reyren, A. Fert, and C. Panagopoulos, Emergent phenomena induced by spin-orbit coupling at surfaces and interfaces, *Nature (London)* **539**, 509 (2016).
- [27] K. G. Wilson, in *New Phenomena in Subnuclear Physics* (Springer, New York, 1977), pp. 69–142.
- [28] S. Hands, A. Kocic, and J. B. Kogut, Four-Fermi theories in fewer than four dimensions, *Ann. Phys.* **224**, 29 (1993).
- [29] S. Hands, Fixed point four Fermi theories, [arXiv:hep-lat/9706018](https://arxiv.org/abs/hep-lat/9706018).

- [30] J. Braun, Fermion interactions and universal behavior in strongly interacting theories, *J. Phys. G: Nucl. Part. Phys.* **39**, 033001 (2012).
- [31] E. Fermi, Versuch einer Theorie der β -Strahlen. i, *Z. Phys.* **88**, 161 (1934).
- [32] Y. Nambu and G. Jona-Lasinio, Dynamical model of elementary particles based on an analogy with superconductivity. i, *Phys. Rev.* **122**, 345 (1961).
- [33] D. J. Gross and A. Neveu, Dynamical symmetry breaking in asymptotically free field theories, *Phys. Rev. D* **10**, 3235 (1974).
- [34] J. Hubbard, Electron correlations in narrow energy bands, *Proc. R. Soc. London A* **276**, 238 (1963).
- [35] K. G. Wilson, Confinement of quarks, *Phys. Rev. D* **10**, 2445 (1974).
- [36] C. Gattringer and C. Lang, *Quantum Chromodynamics on the Lattice: An Introductory Presentation* (Springer Science & Business Media, Berlin, Heidelberg, 2009).
- [37] V. Galitski and I. B. Spielman, Spin-orbit coupling in quantum gases, *Nature (London)* **494**, 49 (2013).
- [38] L. Zhang and X.-J. Liu, in *Synthetic Spin-Orbit Coupling in Cold Atoms* (World Scientific, Singapore, 2018), pp. 1–87.
- [39] R. P. Feynman, Simulating physics with computers, *Int. J. Theor. Phys.* **21**, 467 (1982).
- [40] M. Lewenstein, A. Sanpera, V. Ahufinger, B. Damski, A. Sen, and U. Sen, Ultracold atomic gases in optical lattices: Mimicking condensed matter physics and beyond, *Adv. Phys.* **56**, 243 (2007).
- [41] I. Bloch, J. Dalibard, and S. Nascimbene, Quantum simulations with ultracold quantum gases, *Nat. Phys.* **8**, 267 (2012).
- [42] J. Kogut and L. Susskind, Hamiltonian formulation of Wilson's lattice gauge theories, *Phys. Rev. D* **11**, 395 (1975).
- [43] H. B. Nielsen and M. Ninomiya, Absence of neutrinos on a lattice: (i). Proof by homotopy theory, *Nucl. Phys. B* **185**, 20 (1981).
- [44] H. B. Nielsen and M. Ninomiya, Absence of neutrinos on a lattice: (ii). Intuitive topological proof, *Nucl. Phys. B* **193**, 173 (1981).
- [45] Z. Wu, L. Zhang, W. Sun, X.-T. Xu, B.-Z. Wang, S.-C. Ji, Y. Deng, S. Chen, X.-J. Liu, and J.-W. Pan, Realization of two-dimensional spin-orbit coupling for Bose-Einstein condensates, *Science* **354**, 83 (2016).
- [46] W. Sun, B.-Z. Wang, X.-T. Xu, C.-R. Yi, L. Zhang, Z. Wu, Y. Deng, X.-J. Liu, S. Chen, and J.-W. Pan, Highly Controllable and Robust 2D Spin-Orbit Coupling for Quantum Gases, *Phys. Rev. Lett.* **121**, 150401 (2018).
- [47] B. Song, L. Zhang, C. He, T. F. J. Poon, E. Hajiyev, S. Zhang, X.-J. Liu, and G.-B. Jo, Observation of symmetry-protected topological band with ultracold fermions, *Sci. Adv.* **4**, eaao4748 (2018).
- [48] X.-J. Liu, K. T. Law, and T. K. Ng, Realization of 2D Spin-Orbit Interaction and Exotic Topological Orders in Cold Atoms, *Phys. Rev. Lett.* **112**, 086401 (2014).
- [49] X.-J. Liu, K. T. Law, and T. K. Ng, Erratum: Realization of 2D Spin-Orbit Interaction and Exotic Topological Orders in Cold Atoms, *Phys. Rev. Lett.* **113**, 059901(E) (2014).
- [50] N. Q. Burdick, Y. Tang, and B. L. Lev, Long-Lived Spin-Orbit-Coupled Degenerate Dipolar Fermi Gas, *Phys. Rev. X* **6**, 031022 (2016).
- [51] B. Song, C. He, S. Zhang, E. Hajiyev, W. Huang, X.-J. Liu, and G.-B. Jo, Spin-orbit-coupled two-electron Fermi gases of ytterbium atoms, *Phys. Rev. A* **94**, 061604(R) (2016).
- [52] L. F. Livi, G. Cappellini, M. Diem, L. Franchi, C. Clivati, M. Frittelli, F. Levi, D. Calonico, J. Catani, M. Inguscio, and L. Fallani, Synthetic Dimensions and Spin-Orbit Coupling with an Optical Clock Transition, *Phys. Rev. Lett.* **117**, 220401 (2016).
- [53] S. Kolkowitz, S. Bromley, T. Bothwell, M. Wall, G. Marti, A. Koller, X. Zhang, A. Rey, and J. Ye, Spin-orbit-coupled fermions in an optical lattice clock, *Nature (London)* **542**, 66 (2017).
- [54] S. Bromley, S. Kolkowitz, T. Bothwell, D. Kedar, A. Safavi-Naini, M. Wall, C. Salomon, A. Rey, and J. Ye, Dynamics of interacting fermions under spin-orbit coupling in an optical lattice clock, *Nat. Phys.* **14**, 399 (2018).
- [55] D. Jaksch, C. Bruder, J. I. Cirac, C. W. Gardiner, and P. Zoller, Cold Bosonic Atoms in Optical Lattices, *Phys. Rev. Lett.* **81**, 3108 (1998).
- [56] W. Hofstadter, J. I. Cirac, P. Zoller, E. Demler, and M. Lukin, High-Temperature Superfluidity of Fermionic Atoms in Optical Lattices, *Phys. Rev. Lett.* **89**, 220407 (2002).
- [57] I. Bloch, J. Dalibard, and W. Zwerger, Many-body physics with ultracold gases, *Rev. Mod. Phys.* **80**, 885 (2008).
- [58] G. Jotzu, M. Messer, R. Desbuquois, M. Lebrat, T. Uehlinger, D. Greif, and T. Esslinger, Experimental realization of the topological haldane model with ultracold fermions, *Nature (London)* **515**, 237 (2014).
- [59] C.-Z. Chang, J. Zhang, X. Feng, J. Shen, Z. Zhang, M. Guo, K. Li, Y. Ou, P. Wei, L.-L. Wang *et al.*, Experimental observation of the quantum anomalous Hall effect in a magnetic topological insulator, *Science* **340**, 167 (2013).
- [60] C.-Z. Chang, W. Zhao, D. Y. Kim, H. Zhang, B. A. Assaf, D. Heiman, S.-C. Zhang, C. Liu, M. H. Chan, and J. S. Moodera, High-precision realization of robust quantum anomalous Hall state in a hard ferromagnetic topological insulator, *Nat. Mater.* **14**, 473 (2015).
- [61] A. Bermudez, L. Mazza, M. Rizzi, N. Goldman, M. Lewenstein, and M. A. Martin-Delgado, Wilson Fermions and Axion Electrodynamics in Optical Lattices, *Phys. Rev. Lett.* **105**, 190404 (2010).
- [62] D. B. Kaplan and S. Sun, Spacetime as a Topological Insulator: Mechanism for the Origin of the Fermion Generations, *Phys. Rev. Lett.* **108**, 181807 (2012).
- [63] J. Jünemann, A. Piga, S.-J. Ran, M. Lewenstein, M. Rizzi, and A. Bermúdez, Exploring Interacting Topological Insulators with Ultracold Atoms: The Synthetic Creutz-Hubbard Model, *Phys. Rev. X* **7**, 031057 (2017).
- [64] A. Bermudez, E. Tirrito, M. Rizzi, M. Lewenstein, and S. Hands, Gross-Neveu-Wilson model and correlated symmetry-protected topological phases, *Ann. Phys.* **399**, 149 (2018).
- [65] Y. Kuno, Phase structure of the interacting Su-Schrieffer-Heeger model and the relationship with the Gross-Neveu model on lattice, *Phys. Rev. B* **99**, 064105 (2019).
- [66] E. Tirrito, M. Rizzi, G. Sierra, M. Lewenstein, and A. Bermudez, Renormalization group flows for Wilson-Hubbard matter and the topological Hamiltonian, *Phys. Rev. B* **99**, 125106 (2019).

- [67] G. Roose, N. Bultinck, L. Vanderstraeten, F. Verstraete, K. Van Acoleyen, and J. Haegeman, Lattice regularisation and entanglement structure of the Gross-Neveu model, *J. High Energy Phys.* **07** (2021) 207.
- [68] S. Ryu, A. P. Schnyder, A. Furusaki, and A. W. Ludwig, Topological insulators and superconductors: Tenfold way and dimensional hierarchy, *New J. Phys.* **12**, 065010 (2010).
- [69] D. B. Kaplan, A method for simulating chiral fermions on the lattice, *Phys. Lett. B* **288**, 342 (1992).
- [70] H. So, Induced Chern-Simons class with lattice fermions, *Prog. Theor. Phys.* **73**, 528 (1985).
- [71] M. F. Golterman, K. Jansen, and D. B. Kaplan, Chern-simons currents and chiral fermions on the lattice, *Phys. Lett. B* **301**, 219 (1993).
- [72] S. Sen, Chern insulator transitions with Wilson fermions on a hyperrectangular lattice, *Phys. Rev. D* **102**, 094520 (2020).
- [73] S. Aoki, New phase structure for lattice QCD with Wilson fermions, *Phys. Rev. D* **30**, 2653 (1984).
- [74] S. Sharpe, R. Singleton *et al.*, Spontaneous flavor and parity breaking with Wilson fermions, *Phys. Rev. D* **58**, 074501 (1998).
- [75] S. Coleman, *Aspects of Symmetry: Selected Erice Lectures* (Cambridge University Press, Cambridge, 1988).
- [76] S. Coleman, R. Jackiw, and H. Politzer, Spontaneous symmetry breaking in the $O(N)$ model for large N , *Phys. Rev. D* **10**, 2491 (1974).
- [77] S. Coleman and E. Weinberg, Radiative corrections as the origin of spontaneous symmetry breaking, *Phys. Rev. D* **7**, 1888 (1973).
- [78] In Euclidean anisotropic lattices, dimensionless fields have a symmetric rescaling $\Psi(\mathbf{x}) = \tilde{\Psi}(\mathbf{x})/\sqrt{a_0 a_1 + a_1 a_2 + a_2 a_0}$. This leads to the following dimensionless bare mass $\tilde{m} = ma_1/(1 + \xi_1 + \xi_2)$ with $\xi_1 = a_1/a_0$ and $\xi_2 = a_1/a_2$, and coupling strength $\tilde{g}^2 = (g^2/a_1)\xi_1\xi_2/(1 + \xi_1 + \xi_2)^2$. Additionally, due to the presence of additional doublers in the time direction, there is an additive renormalization $\tilde{m} \rightarrow \tilde{m} - \frac{1}{2}\tilde{g}^2(1 + \xi_1 + \xi_2)^2/\xi_1$. The condensates become dimensionless through $\tilde{\Sigma}_0 = \Sigma_0 a_1/(1 + \xi_1 + \xi_2)$, and $\tilde{\Pi} = \Pi a_1/(1 + \xi_1 + \xi_2)$.
- [79] Only in the isotropic case, $a_1 = a_2 =: a$, and along the symmetric line $(-ma, g^2) = (2, g^2)$, does the scalar condensate vanish for any coupling strength $\Sigma_0(g^2) = 0$, which signals a cancellation of the additive mass renormalizations arising from the two fermion doublers at $\mathbf{k} \in \{(0, \pi/a), (\pi/a, 0)\}$. The lack of additive renormalization in this so-called *central Wilson branch* is not a large- N artifact, which has interesting implications for Monte Carlo studies of other lattice gauge theories [106,107].
- [80] Z. Wang and S.-C. Zhang, Simplified Topological Invariants for Interacting Insulators, *Phys. Rev. X* **2**, 031008 (2012).
- [81] Z. Wang and S.-C. Zhang, Strongly correlated topological superconductors and topological phase transitions via Green's function, *Phys. Rev. B* **86**, 165116 (2012).
- [82] Z. Wang and B. Yan, Topological Hamiltonian as an exact tool for topological invariants, *J. Phys.: Condens. Matter* **25**, 155601 (2013).
- [83] W. Chen, Weakly interacting topological insulators: Quantum criticality and the renormalization group approach, *Phys. Rev. B* **97**, 115130 (2018).
- [84] Z. Wang, X.-L. Qi, and S.-C. Zhang, Topological Order Parameters for Interacting Topological Insulators, *Phys. Rev. Lett.* **105**, 256803 (2010).
- [85] V. Gurarie, Single-particle Green's functions and interacting topological insulators, *Phys. Rev. B* **83**, 085426 (2011).
- [86] D. J. Thouless, M. Kohmoto, M. P. Nightingale, and M. den Nijs, Quantized Hall Conductance in a Two-Dimensional Periodic Potential, *Phys. Rev. Lett.* **49**, 405 (1982).
- [87] At the isotropic point $a_1 = a_2 =: a$, there is an additional $O(2)$ symmetry, such that the parity-broken phase will spontaneously select the direction of the ferromagnetic order in the xy plane. In this limit, one can also envisage the appearance of a Chern-Simons term. However, by its very nature, it can only influence dynamics while our large- N solution focuses on static properties. The dynamical consequences of this term will be studied in the future.
- [88] P. W. Anderson, Antiferromagnetism. Theory of superexchange interaction, *Phys. Rev.* **79**, 350 (1950).
- [89] P. W. Anderson, in *Solid State Physics*, Vol. 14 (Elsevier, New York, 1963), pp. 99–214.
- [90] W. Heisenberg, Zur Theorie des Ferromagnetismus, *Z. Phys.* **49**, 619 (1928).
- [91] Z. Nussinov and J. van den Brink, Compass models: Theory and physical motivations, *Rev. Mod. Phys.* **87**, 1 (2015).
- [92] A. Kitaev, Anyons in an exactly solved model and beyond, *Ann. Phys.* **321**, 2 (2006).
- [93] B. Douçot, M. V. Feigel'man, L. B. Ioffe, and A. S. Iosevich, Protected qubits and chern-simons theories in josephson junction arrays, *Phys. Rev. B* **71**, 024505 (2005).
- [94] D. Bacon, Operator quantum error-correcting subsystems for self-correcting quantum memories, *Phys. Rev. A* **73**, 012340 (2006).
- [95] M. Li, D. Miller, M. Newman, Y. Wu, and K. R. Brown, 2D Compass Codes, *Phys. Rev. X* **9**, 021041 (2019).
- [96] J. Dorier, F. Becca, and F. Mila, Quantum compass model on the square lattice, *Phys. Rev. B* **72**, 024448 (2005).
- [97] H.-D. Chen, C. Fang, J. Hu, and H. Yao, Quantum phase transition in the quantum compass model, *Phys. Rev. B* **75**, 144401 (2007).
- [98] R. Orús, A. C. Doherty, and G. Vidal, First Order Phase Transition in the Anisotropic Quantum Orbital Compass Model, *Phys. Rev. Lett.* **102**, 077203 (2009).
- [99] F. Verstraete and J. I. Cirac, Renormalization algorithms for quantum-many body systems in two and higher dimensions, [arXiv:cond-mat/0407066](https://arxiv.org/abs/cond-mat/0407066).
- [100] J. Jordan, R. Orús, G. Vidal, F. Verstraete, and J. I. Cirac, Classical Simulation of Infinite-Size Quantum Lattice Systems in Two Spatial Dimensions, *Phys. Rev. Lett.* **101**, 250602 (2008).
- [101] H.-C. Jiang, Z.-Y. Weng, and T. Xiang, Accurate Determination of Tensor Network State of Quantum Lattice Models in Two Dimensions, *Phys. Rev. Lett.* **101**, 090603 (2008).
- [102] We have implemented the variational iPEPS algorithms described in [108–110], the accuracy of which relies on a refinement parameter D related to the maximum entanglement content of the *Ansatz*. In practice, increasing D leads to better descriptions of the ground state, and $D = 2$ is the minimum value that captures the effect of quantum correlations.
- [103] D. Sheng, Z.-C. Gu, K. Sun, and L. Sheng, Fractional quantum Hall effect in the absence of Landau levels, *Nat. Commun.* **2**, 389 (2011).

- [104] T. Neupert, L. Santos, C. Chamon, and C. Mudry, Fractional Quantum Hall States at Zero Magnetic Field, *Phys. Rev. Lett.* **106**, 236804 (2011).
- [105] D. B. Kaplan and S. Sen, Fractional Quantum Hall Effect in a Relativistic Field Theory, *Phys. Rev. Lett.* **124**, 131601 (2020).
- [106] T. Misumi and Y. Tanizaki, Lattice gauge theory for the Haldane conjecture and central-branch Wilson fermion, *Prog. Theor. Exp. Phys.* **2020**, 033B03 (2020).
- [107] T. Misumi and J. Yumoto, Varieties and properties of central-branch Wilson fermions, *Phys. Rev. D* **102**, 034516 (2020).
- [108] R. Orús and G. Vidal, Simulation of two-dimensional quantum systems on an infinite lattice revisited: Corner transfer matrix for tensor contraction, *Phys. Rev. B* **80**, 094403 (2009).
- [109] H. N. Phien, J. A. Bengua, H. D. Tuan, P. Corboz, and R. Orús, Infinite projected entangled pair states algorithm improved: Fast full update and gauge fixing, *Phys. Rev. B* **92**, 035142 (2015).
- [110] P. Corboz, Variational optimization with infinite projected entangled-pair states, *Phys. Rev. B* **94**, 035133 (2016).